2025 IEEE/SICE International Symposium on System Integration (SII)
January 21-24, 2025, Munich, Germany

Deformation Analysis and Prediction of Drop-Stitch Reinforced Inflatable Robot Link for 1DOF and 2DOF Motion

*Gangadhara Naga Sai Gubbala [1], Masato Nagashima[1], Hiroki Mori[1,2], Young Ah Seong[3], Hiroki Sato[4], Ryuma Niiyama[5], Yuki Suga[6], Tetsuya Ogata[1,7]

***Abstract*— In this study, we observe the dynamic behavior of an inflatable robot arm with an internally reinforced drop-stitch structure. We examine the deformation during motion of 1 and 2 degrees of freedom (DOF) for an inflatable body. The inflatable robot arm has a soft inflatable body as links and rigid servo actuators as joints. We implemented a sinusoidal motion for inflatable links for various payload conditions and analyzed them using a Motion Capture system. To estimate the dynamic deformation of the balloon in motion, we have defined a Deformation Index (DI) metric. Angle, current of the actuator (servo), and DI are used as input to polynomial regression to predict the end effector position. With this analysis, we can understand the complexity of modeling the nonlinear behavior of inflatable links for multi-DOF motion. We observed DI helps improve the prediction of the end effector position by including deformation information. However, the results demonstrate the limitations of polynomial regression analysis of an internally reinforced inflatable robot arm link.**

***Index Terms*— Soft Robotics; Human-Robot Cooperation/Collaboration; Human-Robot/System Interaction**

I. Introduction

Soft robots have shown potential for safe physical human-robot interaction (pHRI) due to their inherent passive compliance [1]. Within soft robots, inflatable robots provide additional features like compactness and being lightweight, making them suitable as links for constructing a collaborative arm. Being lightweight can help reduce the inertia during motion, resulting in low-impact force for unintended contact with humans and surroundings. Our research focuses on analyzing 1DOF and 2DOF inflatable robots with balloons as links and servo actuators as joints, shown in Fig. 2b. From this combination, we can get enough compliance from the soft body and adequate control from the rigid joints [2]. Inflatable robots can have applications ranging from space exploration due to their lightweight nature [3] to healthcare assistance for rehabilitation [4].

However, the inherent compliance of the inflatable balloon causes difficulty in maintaining shape, stability, and control during motion. Hence, we utilize balloons with internal reinforcement that can help overcome deformations and maintain shape. Sato et al. have shown one such structure with internal reinforcement called ”drop-stitch” can help the balloon to maintain shape even under external force [5]. Generally, inflatable structures with drop-stitch are often used in surfing boards, air mattresses, and portable furniture. We aim to explore the balance between flexibility and stability by incorporating this drop-stitch structure into our robot links. With the combination of inflatable links and rigid joints, we examine the deformation of 1DOF and 2DOF inflatable arm's behavior in sinusoidal motion.

We utilized a Motion Capture system to track real-time shape changes of the inflatable link, allowing us to analyze dynamic deformations. We introduced a Deformation Index (DI) metric to quantify these deformations and compare them with different payloads. We used polynomial regression models to predict the end effector position based on angle, current, and DI as inputs. Our findings show the limitations of polynomial regression and the complexity of nonlinear deformations seen in inflatable links.

In this paper, we first present the construction and design established in our previous work [2] shown in Section III. Then, Section IV shows the details of sinusoidal motion and the Deformation Index. Followed by experimental setup, data collection, and experiments shown in Section V. We utilized the data collected in Section V-B to model polynomial regression, predict end effector positions, and evaluate it in Section VI. Insights from the evaluation are discussed in Section VII. Finally, the conclusion and future work in Section VIII show our research direction. This work presents the following contributions:

1) We have quantified deformations by introducing the Deformation Index (DI) for a drop-stitch reinforced inflatable link.
2) We evaluated the polynomial regression models to predict end effector positions from angle, current, and DI as inputs and showed its limitations.

II. Related Work

A. Design and Applications of Inflatable Robots

Inflatable robots recently have gained traction in soft robotics due to their potential in safe, adaptable, and portable

[1]Gubbala Gangadhara Naga Sai, Masato Nagashima, Hiroki Mori, and Tetsuya Ogata are with the Dept. of Intermedia Art and Science, School of Fundamental Science and Eng., Waseda University, Tokyo 165-8555, Japan. Emails: gangadhara@fuji.waseda.jp, yuuoumaishin@akane.waseda.jp, ogata@waseda.jp, mori@idr.ias.sci.waseda.ac.jp.

[2]Hiroki Mori is also with the Institute for AI and Robotics, Future Robotics Organization, Waseda University, Tokyo 165-8555, Japan.

[3]Young Ah Seong is with the Dept. of System Design, Faculty of Eng. and Design, Hosei University, Tokyo 102-8160, Japan. Email: seong@hosei.ac.jp.

[4]Hiroki Sato is with the School of Project Design, Miyagi University, Miyagi 981-3298, Japan. Email: satoh@myu.ac.jp.

[5]Ryuma Niiyama is with the School of Science and Technology, Meiji University, Tokyo 214-8571, Japan. Email: niiyama@meiji.ac.jp.

[6]Yuki Suga is with Waseda Research Institute for Science and Engineering (WISE), Waseda University, Tokyo 165-8555, Japan. And is also with Sugar Sweet Robotics (SSR). Email: ysuga@ysuga.net.

[7]Tetsuya Ogata is also with the National Institute of Advanced Industrial Science and Technology (AIST), Tokyo 100-8921, Japan.

applications. One of the notable developments of a 2link inflatable manipulator with polyurethane film was built by Sanan et al. [6]. He demonstrated the utility of inflatable structures in robotic applications for healthcare. Another interesting fully inflatable humanoid robot "King Louie" for space applications was built by Gillespie et al. [3] showing the complexity of multi-DOF inflatable systems.

B. Structural and Deformation Analysis

Sato et al. [5] introduced drop-stitch structure in POrtable and Inflatable MObility (POIMO) devices that improve load-bearing capacity while preserving inherent compliance. An inflatable body shows inherent nonlinear deformations that are difficult to model accurately via traditional rigid-body dynamics because of complex dynamic behaviors [7], [8]. Niiyama et al. [9] proposed a model to understand deformation and actuation for inflatable joints stressing the importance of active pressure control in pHRI scenarios. Troise et. al [10] built an inflatable arm for aerospace applications with inflatable tubes and showed the relation between radial deformations and air pressure. Armanini et al. [11] and Longhui et al. [12] reviewed numerical methods for analyzing nonlinear dynamics in soft robots and showed the complexity of modeling soft robots.

C. Dynamic Analysis and Motion Capture

Since soft robots cannot utilize established conventional concepts of robotics, we need to use accurate dynamic tracking systems like Motion Capture. Hofer et al. [13] tracked an inflatable spherical robotic arm using Motion Capture to evaluate their modeling and control. Thuruthel et al. [14] demonstrated effective high-precision external sensing for a soft robotic finger using Motion Capture as ground truth to track the movements. Nazeer et al. [15] evaluated imitation learning for a soft robot using Motion Capture data as a reference showing the potential of combining external sensing. We also utilize Motion Capture data to address the dynamic deformation analysis of internally reinforced inflatable links in motion. Our study aims to find the complexity of the inflatable link by analyzing the dynamic deformations of 1DOF and 2DOF motion while maintaining constant internal pressure.

III. Design and Construction of Inflatable Arm

A. Inflatable body with Drop-stitch

The inflatable body is internally reinforced with a drop-stitch structure and is capable of maintaining shape under external force. Drop-stitch is manufactured by connecting two fabrics with the help of space yarns or threads and these fabrics are coated with thermoplastic polyurethane (TPU). The threads connect the inner surfaces of the fabric as shown in Fig. 1. When an external force is applied to a normal balloon, it bends, tilts, or deforms. But with a drop-stitch balloon, it maintains its shape under external force due to an increase in internal pressure. This occurs as the tension in the threads influences the force distribution on the surface of the balloon. When the drop-stitched balloon bends the volume decreases and pressure increases (PV = Constant), which results in pushing other parts of the balloon apart leading to an increase in the tension in the threads.

Fig. 1: Transparent balloon sample with an internal drop-stitch structure. The top and bottom surfaces are connected by threads or space yarn to help maintain the shape of the balloon under external forces. Bending, titling, or deforming is reduced due to force distribution by the threads.

B. Design and Integration of the Inflatable Link

The design of the Inflatable link is made of cuboidal shape, measuring 95x10x10 cm (length, width, height) as seen in Fig. 2a to analyze its behavior in the cantilever position. We designed the integration of the balloon with actuator (servo) by using a metal plate called a "balloon plate". This balloon plate is glued to a piece of fabric and then it is fixed onto the surface of the balloon via strong adhesive, as shown in Fig. 2b(1, 2, 3). The actuator (Dynamixel Pro Servo motors) is connected to another metal plate called the "mediator plate", which consists of 2 sets of holes, as shown in Fig. 2b(4). Now the outer set of holes is screwed to the balloon plate, and the inner set of holes to the actuator as shown in Fig. 2b(5). In

(a) Balloon dimension

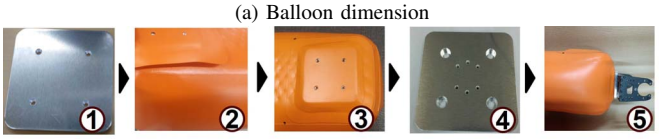

(b) Actuator attachment process [2].

Fig. 2: (a) Inflatable balloon link dimensions are 950mm x 150mm x 150mm. To analyze its behavior in the cantilever position we use the cuboidal shape. (b) Process for attaching the actuator on the inflatable balloon link. (1)With an adhesive the balloon plate (1) is fixed to a fabric piece(2), then attached to the balloon (3). Another metal plate called "mediator plate" (4), connects the soft body (inflatable link) with the rigid joint (servo frame) (5).

our previous research, Gubbala et al. [2] realized that the top-bottom balloon configuration has the best resilience and recovery to its original position after payload tests as shown in Fig. 3. Hence, we choose top-bottom orientation for the design of 1DOF and 2DOF links.

C. 1DOF and 2DOF Link Design

1DOF and 2DOF inflatable actuator orientations are designed to allow simple to and fro motion that can help us get

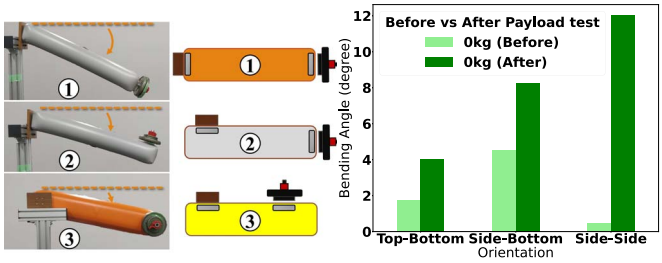

(a) Payload test(PT) (b) Before and After Evaluation

Fig. 3: (a) This shows three orientations for testing balloon resilience: top-bottom, side-bottom, and side-side. We apply a payload to see how well the balloon returns to its original shape in each position. The balloon orientations are (1) top-bottom, (2) side-bottom, and (3) side-side. (b) This graph compares the balloon's bending angle before and after the payload test for different orientations. The y-axis shows the bending angle in degrees. The top-bottom orientation shows the least deformation, indicating the best resilience. This plot is taken from our previous research[2]

dynamic deformations under different payload conditions. Fig. 4 shows stick figure representations of these designs.

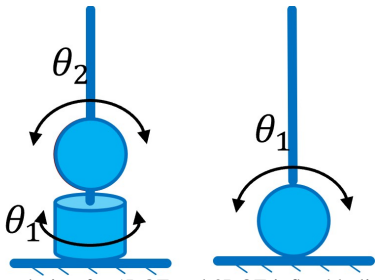

Fig. 4: Stick figure design for 1DOF and 2DOF inflatable links. The 1DOF design oscillates in a single plane, while the 2DOF design allows movement in two planes, enabling more complex motions for dynamic analysis.

IV. Methods

In this section, we discuss the methods for analyzing the inflatable link in motion. Sinusoidal motion is applied to the link for to and fro motion, and then we define the Deformation Index (DI) as a metric to quantify the deformations.

A. Sinusoidal Motion of the Inflatable Link

When a soft body undergoes sinusoidal motion, due to gradual increase and decrease in the speed, the inflatable link can minimize deformations. This approach is used by Huang et al. [16] and Sun et al. [17] to ensure structural integrity during operation for soft bodies.

For the 1DOF setup, the link θ_1 is rotated from +30° to -30° in the x-z plane, completing two full cycles. Where one cycle is defined as 0° to -30° to 0° to +30° to 0°. In 1 cycle we have 256 steps, where each step takes 17ms, giving us a frequency of 59Hz. The whole system's motion frequency is 0.23 Hz. Similarly in 2DOF configuration servo motors θ_1, θ_2 move in both the x-z and x-y planes making a more complex trajectory by completing 2 full cycles. For this research, speed is kept constant corresponding to the operating frequency and to study the inflatable body behavior.

B. Deformation Index for Inflatable Link

We have quantified the overall deformation of the inflatable link during motion by defining the Deformation Index (DI). It measures the relative change in deformation from the initial state (t = 0) at various positions along the link. We compute this by calculating the change in length as shown in this equation:

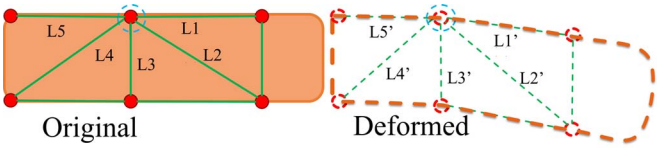

Fig. 5: Deformation Index (DI) is the mean relative error in length. Calculation is done by comparing the original length L_i to the deformed length L_i' at different points along the link.

$$\mathrm{DI}(L) = \frac{1}{N}\sum_{n=1}^{N}\left(\frac{|L_i - L_i'|}{L_i}\right) \quad (1)$$

L_i is the original length and L_i' is the deformed length. The change is in modulus for getting a positive value. N is the number of markers on the inflatable link. The total sum of the change in length across all markers is normalized by N to get the deformation index. With this approach, we can get DI for the whole link and it can be compared for various loads for the same motion pattern.

V. Experiments

In this section, we first show the experimental setup to conduct the Motion Capture (MoCap) experiments and collect the data while the inflatable robot is in sinusoidal motion. The internal pressure of the inflatable link is kept at 6 PSI (41.3kPa) and is tightly sealed.

A. Experimental Setup

The inflatable link's actuators are mounted on an aluminum frame for stability. We placed the setup in a MoCap studio with high-speed IR cameras of 240 Hz frequency. Reflective markers are fixed onto the link along the longest edges with a total of 16 markers placed as shown in Fig. 6. This distribution allowed thorough tracking of the link's deformation.

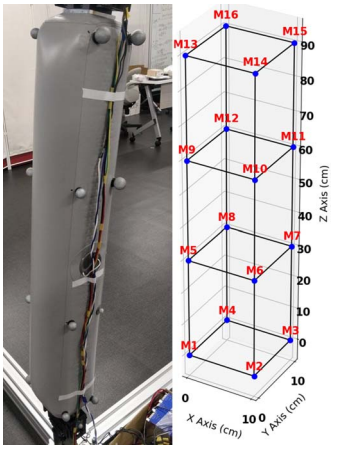

Fig. 6: Inflatable link is attached with 16 reflective markers, that are evenly spaced along the link's edges, allowing precise tracking of deformation during motion.

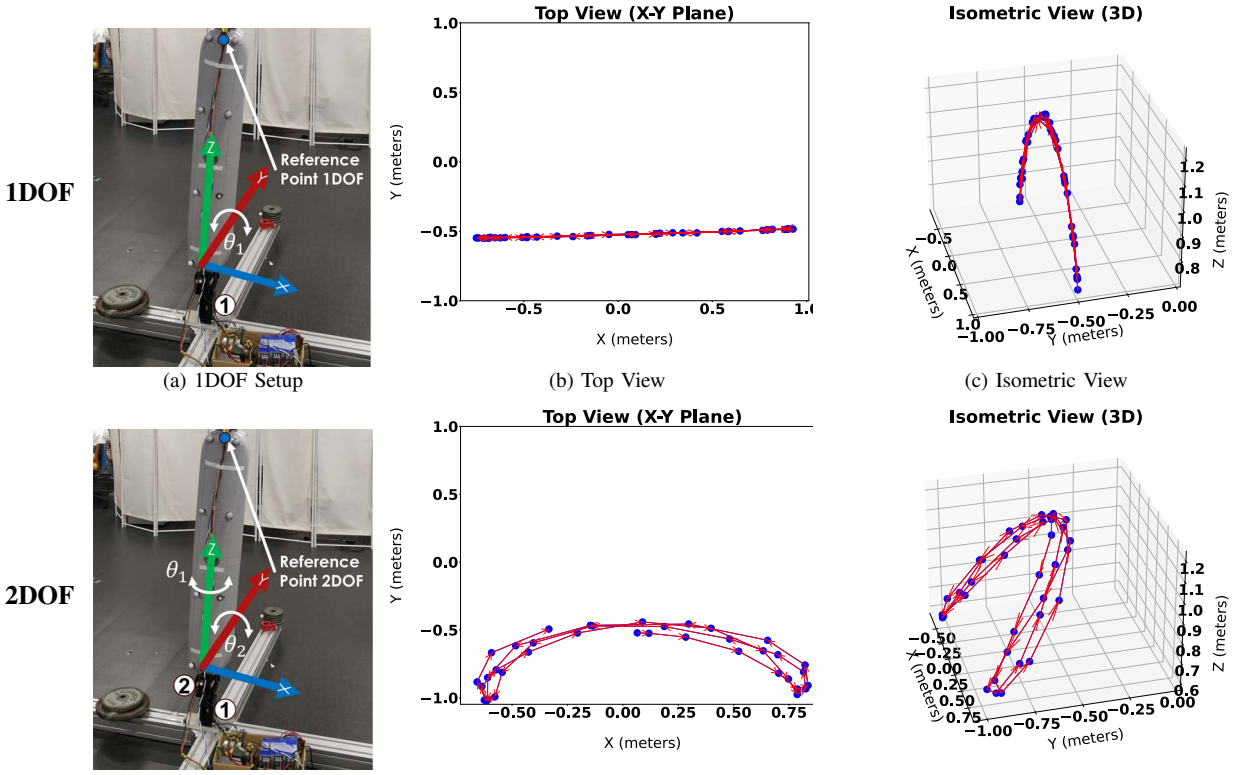

(a) 1DOF Setup (b) Top View (c) Isometric View

(d) 2DOF Setup (e) Top View (f) Isometric View

Fig. 7: 1DOF and 2DOF setups vs end effector position plotted in different perspectives of the top view and isometric view. Blue dots show the reference point of end effector. The top view for 1DOF motion shows straight line motion, where as the 2DOF top view shows a more complex pattern. 3D view for 1DOF is an expected arc but adding another second joint makes 2DOF shift its extreme positions and move in 3D space.

B. Motion Capture Experiment

We performed 2 cycles of sinusoidal motion for 1DOF and 2DOF and collected angle, and current data for 512 steps. We also collected the Motion Capture (MoCap) data as x,y,z coordinates for the markers shown in Fig. 6. Each motion of 1DOF and 2DOF has payloads of 0, 0.5, 1, 1.5, and 2 Kgs. We used barbell weights at the top of the inflatable link and fixed it with a barbell clip onto the rod screwed to the balloon. For both 1DOF and 2DOF motion, the servos are moved from 0° to -30° to +30° to -30° back to 0°, which is considered as 2 cycles. In 1DOF, the servo is moved in x-z plane, whereas in 2DOF the servos are moved in x-z and z-y planes as shown in Fig. 7. We have plotted the end effector position from different views to understand the motion. For example, 2DOF motion with a 2Kg payload is shown in Fig. 8 with images at every 30° angle change.

C. Deformation Index Analysis

From the data captured using MoCap studio, we calculated the length between markers using Euclidean distance. Then we input these lengths into the Deformation Index (DI) Equation 1 for both 1DOF and 2DOF motion setups. To understand the real-time deformation for a given step in the motion, we have plotted the DI in a series of images showing the behavior of bending in Fig. 8. Next, we plotted DI for 512 steps for all the payloads at their corresponding angle for 1DOF and 2DOF setups for corresponding trial 1. For the 1DOF setup, the DI plot is shown in Fig. 9 and Similarly, the 2DOF plot is shown in Fig. 10.

Trial 2 has a similar structure of DI of trial 1. Now to check the correlation between DI and DOF, we plot mean DI vs time steps for comparing 1DOF and 2DOF setups as shown in Fig. 11 which confirms the complexity increases as DOF increases.

VI. Prediction and Evaluation of End Effector Positions

A. Predicting end effector Positions

Estimating the end effector position for an inflatable robot arm is quite challenging due to its deformations; traditional inverse kinematics cannot be applied directly. Hence, we utilize the previously collected data as input features like actuator angles, actuator currents, and the deformation index, to model a nonlinear relationship using polynomial regression to predict the end effector positions E_X, E_Y, and E_Z.

1DOF system's input features are the actuator angle A_1, actuator current C_1, and the deformation index DI. 2DOF system's input features are actuator angles A_1 and A_2, actuator currents C_1 and C_2, and the deformation index DI. We define the polynomial regression for the 1DOF system predicting E_X, E_Y, and E_Z at polynomial degree d (from 1 to 6) as:

$$\hat{E}_i = \sum_{\substack{j+k+l \le d \\ j,k,l \ge 0}} \beta_{jkl}^{(i)} (A_1)^j (C_1)^k (DI)^l, \quad d \in [1,6] \qquad (2)$$

In the above equation for $i \in \{X, Y, Z\}$, $\beta_{jkl}^{(i)}$ are the coefficients for each term. Similarly, for the 2DOF system

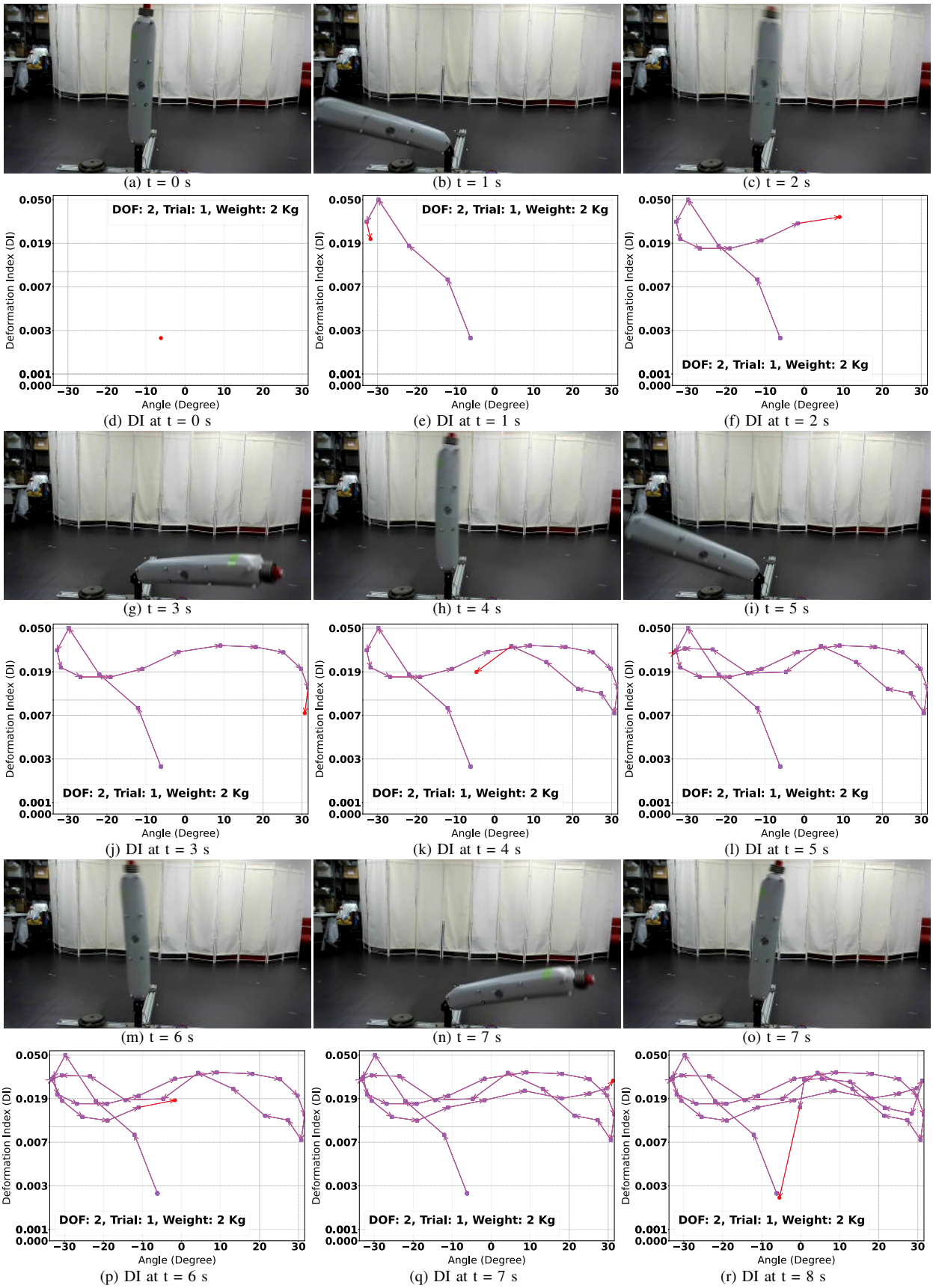

(a) t = 0 s (b) t = 1 s (c) t = 2 s

(d) DI at t = 0 s (e) DI at t = 1 s (f) DI at t = 2 s

(g) t = 3 s (h) t = 4 s (i) t = 5 s

(j) DI at t = 3 s (k) DI at t = 4 s (l) DI at t = 5 s

(m) t = 6 s (n) t = 7 s (o) t = 7 s

(p) DI at t = 6 s (q) DI at t = 7 s (r) DI at t = 8 s

Fig. 8: Time-lapse of 2DOF motion with 2kg payload. Images show link position at 1-second intervals. Below each image is a corresponding plot of the DI vs. angle. This shows the deformation changes throughout one cycle till t = 4, then the second cycle starts. The red arrow in each Deformation Index (DI) plot is the current position of the robot

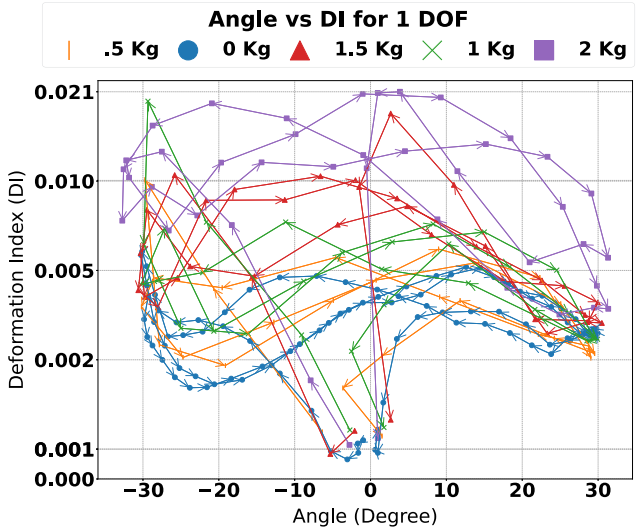

Fig. 9: 1DOF setup, where Deformation index (DI) (y-axis) vs. Angle (x-axis, from $-30°$ to $+30°$) is plotted. With the increase in payload from 0 kg to 2 kg, DI also increases. It is observed that negative angles result in more deformation than positive angles due to the inherent shape that is bent towards the positive side. There is a delayed response present in the system causing hysteresis, particularly at higher payloads due to deformations.

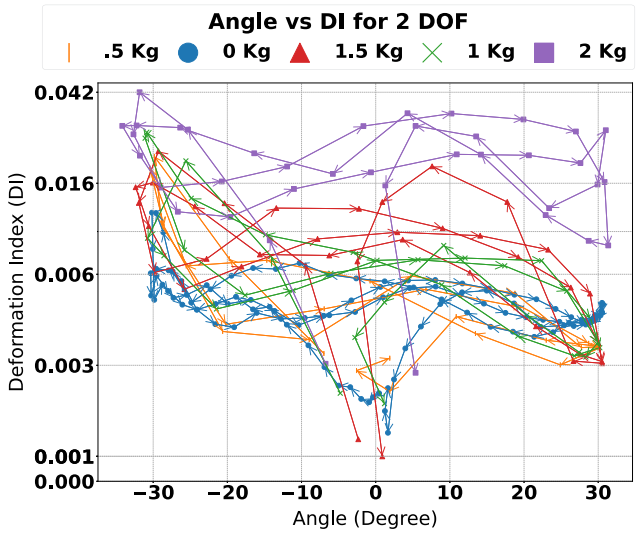

Fig. 10: 2DOF setup, where the Deformation index (DI) (y-axis) vs. Angle (x-axis, from $-30°$ to $+30°$) is plotted. The inflatable link deforms more compared to the 1DOF setup because of deformation in multiple planes. The recovery after bending is difficult as the link remains in an extreme position until the material is stretched, causing hysteresis at higher angles and loads.

at polynomial degree d (from 1 to 6), the regression model is given by:

$$\hat{E}_i = \sum_{\substack{j+k+l+m+p \le d \\ j,k,l,m,p \ge 0}} \beta^{(i)}_{jklmp} (A_1)^j (A_2)^k (C_1)^l (C_2)^m (DI)^p \tag{3}$$

Where in the above equation, $d \in [1, 6]$, $i \in \{X, Y, Z\}$, and $\beta^{(i)}_{jklmp}$ are the coefficients for each term.

B. Evaluation with Euclidean Distance

To assess the prediction of the polynomial model, we utilize Euclidean distance to measure the error between the actual and predicted values. In the below equations, $E_{X,s}, E_{Y,s}, E_{Z,s}$ are the actual and $\hat{E}_{X,s}, \hat{E}_{Y,s}, \hat{E}_{Z,s}$ are the

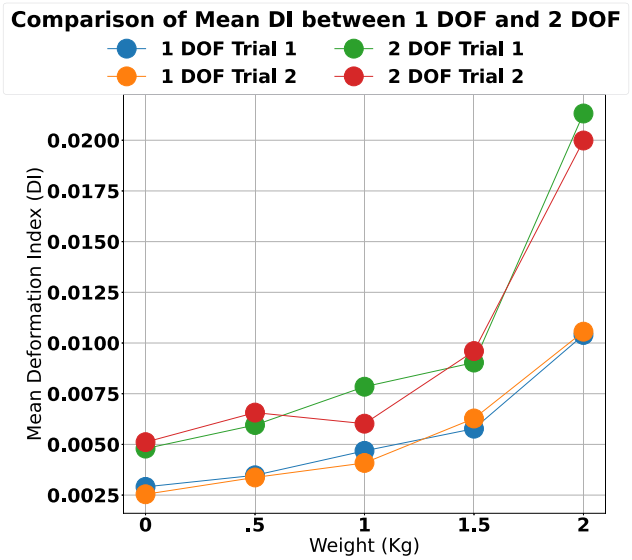

Fig. 11: Mean deformation index (DI) vs. Payloads for 1DOF and 2DOF motion is plotted. The 2DOF setup has higher DI consistently than the 1DOF setup for all payloads. Both exhibit higher deformation with an increase in loads, but the 2DOF system is more sensitive to deformation.

predicted end effector positions. The error in each direction is defined as:

$$dx_s = (E_{X,s} - \hat{E}_{X,s}) \tag{4}$$

$$dy_s = (E_{Y,s} - \hat{E}_{Y,s}) \tag{5}$$

$$dz_s = (E_{Z,s} - \hat{E}_{Z,s}) \tag{6}$$

The Euclidean distance (ED) for a sample is given by:

$$ED_s = \sqrt{dx_s^2 + dy_s^2 + dz_s^2} \tag{7}$$

For a given degree of freedom and its payload, we define the net deformation as Mean Euclidean Distance (Mean ED), which is the average of the Euclidean distance across S samples (with $S = 512$ steps)

$$\text{Mean ED} = \frac{1}{S} \sum_{s=1}^{S} ED_s \tag{8}$$

We verified the generalization of the polynomial regression models by training models on trial 1 data and then testing models on trial 2. To overcome overfitting, we used 5-fold cross-validation and used Euclidean distance as an evaluation metric. In Fig. (12, 13), we plotted Euclidean distance error vs. time for all polynomial degrees 1 to 6. In these plots, the linear model has higher error indicating the system's nonlinear behavior.

Next, we plot the overall mean Euclidean distance for polynomial degrees 1 to 6 for both the 1DOF and 2DOF systems in Fig. 14. For the 1DOF system, degree 5 has the lowest error, and for the 2DOF system, degree 3 is the lowest error. Even though 2DOF motion is complex, having additional inputs such as A_1, A_2, C_1, C_2, and DI, compared to 1DOF with only A_1, C_1 and DI helps it generalize 2DOF at a lower degree.

C. Significance of Deformation Index (DI) for Prediction

To check if DI contributes to improving the prediction of the end effector position for polynomial regression we set

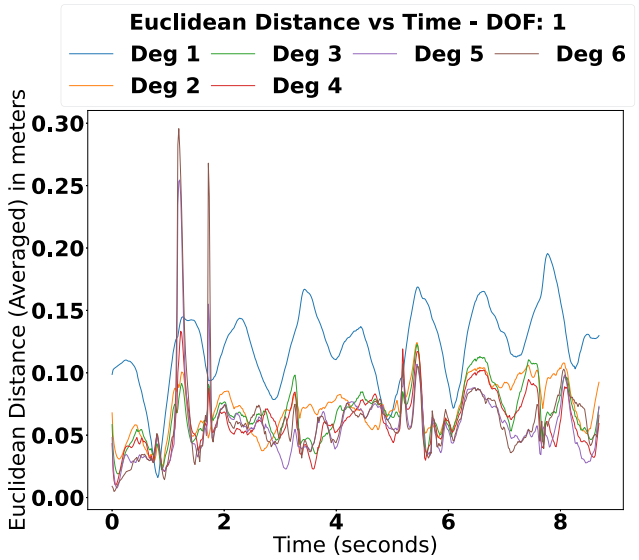

Fig. 12: Euclidean distance error vs time for the 1DOF is plotted with polynomial degrees 1 to 6. Polynomial degree 1 always shows high error. Spikes are seen for degree 6 because of possible overfitting. Degree 5 seems to have a lower error as it is seen at the bottom.

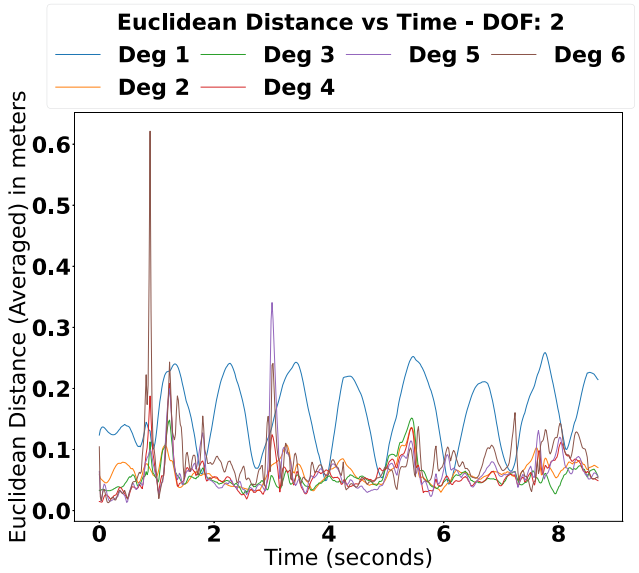

Fig. 13: Euclidean distance error vs. time for the 2DOF is plotted with polynomial degrees 1 to 6. Polynomial degree 1 has the highest error, while higher degrees such as 5 and 6 show sharp spikes, indicating potential overfitting. Degree 3 achieves the lowest overall Euclidean distance error.

$DI = 0$ and train the models. When $DI = 0$ it indicates the balloon did not change its shape and check the influence of DI on the polynomial models. This helps us to compare the prediction of the polynomial model's end effector position with and without DI, for 1DOF and 2DOF setups. Fig. 15 shows the comparison of the mean Euclidean distance. In all the cases, with DI improves the model's performance by reducing the prediction error compared to models trained without DI.

With the addition of DI, models gain deformation insights to help predict the end effector position accurately. DI is currently calculated from Motion Capture, but by calculating DI with the relative change of the inflatable body, we can utilize DI as a system variable to predict the robot's motion.

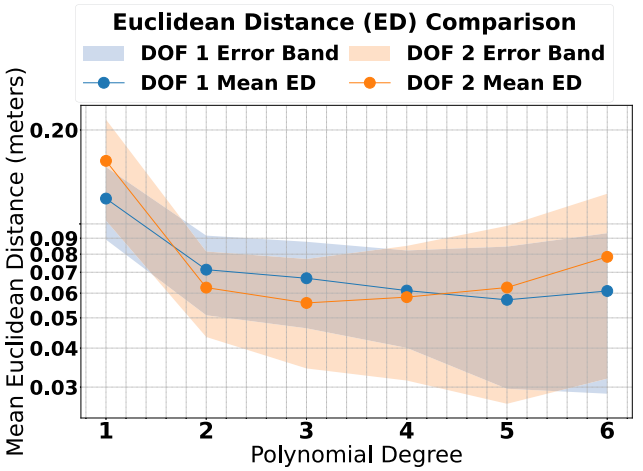

Fig. 14: Comparison of Mean Euclidean distance vs. polynomial degrees 1 to 6 for 1DOF and 2DOF systems is plotted. The 1DOF setup has the least error at degree 5 and the 2DOF at degree 3. After the lowest error, as the polynomial degree increases, the error also increases due to overfitting. At degree 1, the highest error is observed, establishing the nonlinear relationship in the data. Standard deviation error bands are plotted to show data variation.

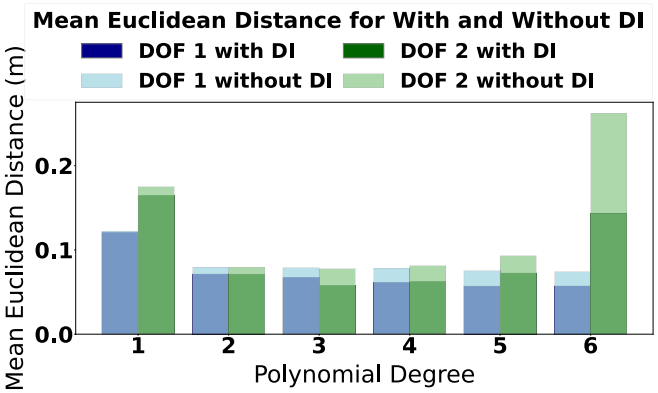

Fig. 15: Comparison of mean Euclidean distance for 1DOF and 2DOF setups with and without DI for polynomial degrees from 1 to 6. Training with DI shows consistency in reducing the error for both 1DOF and 2DOF setups, indicating its importance in improving prediction accuracy for inflatable body links.

VII. Discussion

The limitations of modeling the behavior of inflatable robot links using polynomial regression are discussed in this section. For 1DOF and 2DOF setups, lower polynomials showed higher errors up to an optimal degree, then higher polynomials are prone to overfitting and errors have increased. Also, the limitation of polynomial regression can be seen as the complexity of the model grew from 1DOF to 2DOF, the error got higher, and the 2DOF model started to overfit from earlier degrees. This shows polynomial models have difficulty in capturing the inflatable robot's behavior.

Our observations of increased system complexity with higher DOF align with Armanini et al. [11] increased complexity of multi-DOF soft manipulators. Polynomial regression is a preliminary test for modeling inflatable links, adopting more advanced techniques suggested by Santina et al. [18] about combining model-based and learning-based methods like recurrent neural networks can be beneficial. The optimal polynomial degree selected in this study is based

on the test data (trial 2) used in this study. We think a more extended dataset would benefit further analysis of such complex models, as suggested by Santina et al.

The significance of the Deformation Index (DI) is shown by the improvement of prediction accuracy of end effector position compared to models trained without DI. Models that included DI had lower Euclidean distance consistently across all the polynomials. Gubbala et al. [2] have utilized a similar drop-stitch reinforced inflatable robot arm with machine learning for wiping tasks. However, exploring more generalized methods, such as predicting the end effector position, would benefit multiple applications.

VIII. Conclusion and Future Work

In this paper, we evaluated the end effector positions for an inflatable robot link using polynomial regression. The models were trained using angle, current, and Deformation Index (DI) to predict the end effector positions for 1DOF and 2DOF sinusoidal motion under different payload conditions. The 1DOF setup achieved the lowest Euclidean distance error at degree 5, and the 2DOF setup at degree 3. This is due to the additional inputs A_1, A_2, C_1, C_2, and DI, which provided more information to capture the system's complex dynamics. However, polynomial regression showed performance limitations at higher degrees due to overfitting.

The comparison of prediction for polynomial models trained with and without DI has shown the effectiveness of DI for capturing the nonlinear behavior of an inflatable robot system. On the other hand, as the polynomial degree increased, sharp spikes were observed in prediction values due to the overfitting of train data.

Our future work should explore machine learning methods like neural networks or recurrent neural networks that are proven to handle complex nonlinear behaviors. Calculating DI directly with alternatives to Motion Capture, such as from soft sensors or flex sensors can help improve the applications in real-world scenarios. Additionally, integrating models that are in real-time could increase stability and responsiveness, making them suitable for applications in physical human-robot collaboration and space exploration robotics due to their lightweight and compact size.

References

[1] D. Rus and M. T. Tolley, "Design, fabrication, and control of soft robots," *Nature*, vol. 521, no. 7553, pp. 467–475, 2015.

[2] G. N. S. Gubbala, M. Nagashima, H. Mori, *et al.*, "Augmenting compliance with motion generation through imitation learning using drop-stitch reinforced inflatable robot arm with rigid joints," *IEEE RA-L*, vol. 9, no. 10, pp. 8595–8602, 2024.

[3] M. T. Gillespie, C. M. Best, and M. D. Killpack, "Simultaneous position and stiffness control for an inflatable soft robot," in *Proc. IEEE Int. Conf. Robot. Autom. (ICRA)*, 2016, pp. 1095–1101.

[4] R. Gassert and V. Dietz, "Rehabilitation robots for the treatment of sensorimotor deficits: A neurophysiological perspective," *J. Neuroeng. Rehabil.*, vol. 15, no. 1, pp. 1–15, 2018.

[5] H. Sato, Y. Seong, R. Yamamura, *et al.*, "Soft yet strong inflatable structures for a foldable and portable mobility," *Ext. Abstr. CHI Conf. Hum. Factors Comput. Syst.*, 2020.

[6] S. Sanan, P. S. Lynn, and S. T. Griffith, "Pneumatic torsional actuators for inflatable robots," *J. Mech. Robot.*, vol. 6, 2014.

[7] G. S. Chirikjian, "Conformational modeling of continuum structures in robotics and structural biology: A review," *Adv. Robot.*, vol. 29, no. 13, pp. 817–829, 2015.

[8] H. Mochiyama and H. Kobayashi, "The shape jacobian of a manipulator with hyper degrees of freedom," in *Proc. IEEE Int. Conf. Robot. Automat.*, vol. 4, 1999, pp. 2837–2842.

[9] R. Niiyama, Y. Seong, Y. Kawahara, and Y. Kuniyoshi, "Blower-powered soft inflatable joints for physical human-robot interaction," *Front. Robot. AI*, vol. 8, 2021.

[10] M. Troise, M. Gaidano, P. Palmieri, *et al.*, "Static modeling of an inflatable robotic arm for aerospace applications," in *Adv. Service Ind. Robot.* Ser. Mech. Mach. Sci. A. Müller and M. Brandstötter, Eds., vol. 120, Springer, Cham, 2022, pp. 474–481.

[11] C. Armanini, F. Boyer, A. T. Mathew, C. Duriez, and F. Renda, "Soft robots modeling: A structured overview," *IEEE Trans. Robot.*, vol. 39, no. 3, pp. 1728–1748, 2023.

[12] L. Qin, Z. Zhang, X. Xu, *et al.*, "Modeling and simulation of dynamics in soft robotics: A review of numerical approaches," *Soft Robot.*, vol. 10, no. 3, pp. 431–455, 2023.

[13] M. Hofer and R. D'Andrea, "Design, fabrication, modeling and control of a fabric-based spherical robotic arm," *Mechatronics*, vol. 68, 2020.

[14] T. G. Thuruthel, B. Shih, C. Laschi, and M. T. Tolley, "Soft robot perception using embedded soft sensors and recurrent neural networks," *Sci. Robot.*, vol. 4, no. 26, eaav1488, 2019.

[15] M. S. Nazeer, C. Laschi, and E. Falotico, "Soft dagger: Sample-efficient imitation learning for control of soft robots," *Sensors*, vol. 23, p. 8278, 2023.

[16] W. Huang, X. Huang, C. Majidi, *et al.*, "Dynamic simulation of articulated soft robots," *Nat. Commun.*, vol. 11, p. 2233, 2020.

[17] Y. Sun, A. Abudula, H. Yang, *et al.*, "Soft mobile robots: A review of soft robotic locomotion modes," *Curr. Robot. Rep.*, pp. 1–27, 2021.

[18] C. D. Santina, C. Duriez, and D. Rus, "Model-based control of soft robots: A survey of the state of the art and open challenges," *IEEE Control Syst. Mag.*, vol. 43, no. 3, pp. 30–65, 2023.